REPORT DOCUMENTATION PAGE

Form Approved
OMB No. 0704-0188

1. REPORT DATE *(DD-MM-YYYY)*	2. REPORT DATE	3. DATES COVERED *(From - To)*
	June 25, 2001	Interim Report

4. TITLE AND SUBTITLE

Structural and Electrochemical Properties of Amorphous and Crystalline Molybdenum Oxide Aerogels

5a. CONTRACT NUMBER

5b. GRANT NUMBER

N00014-93-1-0245

5c. PROGRAM ELEMENT NUMBER

PR No: 01PR0086-00

6. AUTHOR(S)

W. Dong, A. N. Mansour and B. Dunn

5d. PROJECT NUMBER

5e. TASK NUMBER

5f. WORK UNIT NUMBER

7. PERFORMING ORGANIZATION NAME(S) AND ADDRESS(ES)

Bruce S. Dunn
Department of Materials Science and Engineering
University of California, Los Angeles
Los Angeles, CA 90095

8. PERFORMING ORGANIZATION REPORT NUMBER

Technical Report #18

9. SPONSORING/MONITORING AGENCY NAME(S) AND ADDRESS(ES)

Office of Naval Research
800 North Quincy Street
Arlington, VA 22217

10. SPONSOR/MONITOR'S ACRONYM(S)

11. SPONSORING/MONITORING AGENCY REPORT NUMBER

12. DISTRIBUTION AVAILABILITY STATEMENT

Reproduction in whole, or in part, is permitted for any purpose of the United States Government.
This document has been approved for public release and sale; its distribution is unlimited.

13. SUPPLEMENTARY NOTES

Submitted for publication in: *Solid State Ionics*

14. ABSTRACT

The structure and chemical differences among amorphous, crystalline and nanocrystalline molybdenum oxide aerogels were determined using EXAFS, FTIR and XRD. These different forms of the same nominal material are produced by heat treatment. The influence of the structural differences on electrochemical properties was examined using stepped cyclic voltammetry. The most interesting material was the MoO_3 aerogel heated to 300 °C. The material was found to be nanocrystalline; there are no XRD peaks but the EXAFS were virtually identical to orthorhombic MoO_3. The electrochemcial response of the nanocrystalline material contains characteristics of both the amorphous and crystalline forms, but with better lithium capacity than either one.

15. SUBJECT TERMS

molybdenum oxide, aerogel, electrochemical properties, EXAFS

16. SECURITY CLASSIFICATION OF:			17. LIMITATION OF ABSTRACT	18. NUMBER OF PAGES	19a. NAME OF RESPONSIBLE PERSON
a. REPORT	b. ABSTRACT	c. THIS PAGE			19b. TELEPONE NUMBER *(Include area code)*
U	U	U		25	

Standard Form 298 (Rev. 8-98)
Prescribed by ANSI-Std Z39-18

OFFICE OF NAVAL RESEARCH

GRANT: N00014-93-1-0245
R&T Code: 4133041
PR Number: 01PR00860-00

Dr. Richard Carlin

Technical Report #18

Structural and Electrochemical Properties of Amorphous and Crystalline Molybdenum Oxide Aerogels

By

W. Dong, A. N. Mansour and B. Dunn

Submitted for publication in:
Solid State Ionics

Department of Materials Science and Engineering
University of California, Los Angeles
Los Angeles, CA 90095-1595

June 25, 2001

Structural and Electrochemical Properties of Amorphous and Crystalline Molybdenum Oxide Aerogels

W. Dong [a], A.N. Mansour [b], and B. Dunn [a, *]

[a] University of California, Los Angeles, Department of Materials Science and Engineering, Los Angeles, CA 90095

[b] Naval Surface Warfare Center, Carderock Division, 9500 MacArthur Boulevard, West Bethesda, MD 20817-5700

* Corresponding author: Fax: (310) 206-7353; Email address: bdunn@ucla.edu

Abstract

The structure and chemical differences among amorphous, crystalline and nanocrystalline molybdenum oxide aerogels were determined using EXAFS, FTIR and XRD. These different forms of the same nominal material are produced by heat treatment. The influence of the structural differences on electrochemical properties was examined using stepped cyclic voltammetry. The most interesting material was the MoO_3 aerogel heated to 300 °C. The material was found to be nanocrystalline; there are no XRD peaks but the EXAFS were virtually identical to orthorhombic MoO_3. The electrochemcial response of the nanocrystalline material contains characteristics of both the amorphous and crystalline forms, but with better lithium capacity than either one.

Keywords: Molybdenum oxide; Aerogel; Electrochemical properties; EXAFS.

1. Introduction

Crystalline molybdenum trioxide has a two-dimensional layered structure that has been shown to have interesting lithium intercalation properties. [1] [2] Both its open structure and the ease of creating oxygen vacancies in the structure make it an ideal candidate for lithium secondary batteries [3] [4] and electrochromic windows [5]. Lithium capacity of up to 1.5 Li/Mo and discharge capacity of over 300 mAh/g have been reported. [6], [7], [8]

Sol-gel synthesis of MoO_3 is desirable because the low synthesis temperatures can lead to the formation of amorphous or metastable phases not available through traditional synthesis methods. The low temperature phase can exhibit properties that are substantially different from the crystalline phase. Although it is often assumed that lithium intercalation occurs between the 2-D layers of the crystalline MoO_3, previous experiments have not been able to show a direct correlation between the degree of crystallinity and the Li capacity of MoO_3. [9] Even more interesting is that certain amorphous molybdenum oxides have exhibited better intercalation behavior compared to that of crystalline MoO_3. [10] [11] The present paper explores the structure differences among amorphous, crystalline, and nano-crystalline molybdenum oxide aerogels synthesized through the sol-gel process, where heat treatments are able to produce these different forms of the same nominal material. A combination of X-ray absorption fine structure (EXAFS), Fourier transform infrared (FTIR) analysis, and powder X-ray diffraction (XRD) provide detailed insight concerning the chemical and structural nature of these materials. The influence of the structural differences on electrochemical properties of these samples is examined using stepped cyclic voltammetry. This method is an effective means of identifying the contribution of each electroactive species for systems containing more than one redox-active species.

2. Experimental

Molybdenum trioxide aerogels were prepared using molybdenum alkoxides, acetonitrile, nitric acid, and water. Two molybdenum alkoxides were used, molybdenum isopropoxide ($Mo(OC_3H_7)_5$, Alpha Aesar) and molybdenum trichloride isopropoxide ($MoCl_3(OC_3H_7)_2$, Chemat Technology, Inc.), both of which were dissolved in isopropanol. The isopropanol was removed through vacuum evaporation and replaced with acetonitrile (CH_3CN, Aldrich Chemical Co.). Nitric acid and water were then added with vigorous stirring to form the final sol. The preparation of MoO_3 aerogels has been previously detailed. [12] The resulting aerogels were heat-treated in vacuum for 10 hours at 150 (sample A), 300 (sample B), and 400°C (sample C).

FTIR measurements (Nicolet, 510P) were used to establish the types of bonds present for the different samples. Powder x-ray diffraction (XRD) measurements were performed on a Rigaku diffractometer in reflection mode. EXAFS analysis was used to probe the oxidation state and local environment of the Mo ion. The EXAFS experiments were conducted on beamline X11-A at the National Synchrotron Light Source (NSLS) with the electron storage ring operating at an electron energy of 2.8 GeV and a current in the range 110-240 mA. [13] EXAFS spectra were collected in the transmission mode using Si(311) double crystal monochromator with 10% detuning. The energy resolution for this monochromator at the Mo K-edge energy is estimated to be 4.7 eV, which is reasonable when compared to the Mo K-edge core hole natural line width of 4.5 eV. The X-ray intensities were monitored using ionization chambers filled with appropriate mixtures of nitrogen and argon gases. A 15 μm thick Mo foil was used as an internal reference for energy calibration and subsequent calibration of the EXAFS amplitudes. The EXAFS spectra were taken at room temperature (RT) and near the temperature of liquid nitrogen (LN). The x-ray absorption edge jump ($\Delta\mu x$) for each sample is listed in Table I. Fits for the oxide samples were performed in the r-space range 1.10 - 2.09 Å using the FEFFIT Code. [14] The Fourier transform (FT) data were generated using k^3-weighted EXAFS spectra over the k-space range 2.25 - 15.45 $Å^{-1}$. The fit for the Mo foil was made in the r-space 1.60-3.60 Å using Fourier

transform generated with k^3-weighted EXAFS data over the k-space range 2.35-17.55 $Å^{-1}$. The photoelectron wave number, k, was defined by assigning the edge energy to the inflection point above the pre-edge peak. (Table 1)

The electrochemical behavior was determined for a crushed aerogel mixed with conductive carbon powder (80:15 weight ratio, respectively). An additional 5% of the mass was contributed by the polyvinylidene fluoride (PVDF) binder. The mixture was suspended in solvent (N-methyl-2 pyrrolidone) and cast onto a stainless steel mesh current collector. The resulting electrode was heat-treated at 120°C under vacuum to remove the solvent and adsorbed water. Cyclic voltammetry (CV) was carried out using a three-electrode cell with the MoO_3 as the working electrode and lithium foil as the counter and reference electrodes. $LiClO_4$ (1M) in propylene carbonate (PC) served as the electrolyte. The voltage was swept at a rate of 0.1 mV/sec from the open circuit (OC) voltage to various potentials, with the lowest being 1.5 V.

3. Results

The chemical composition of the aerogels was determined through thermogravimetry (TG, Dupont 9900 thermal analysis system) measurements in combination with chemical analysis (Texas Analytical Laboratories). The as-prepared molybdenum oxide aerogels are actually hydrated molybdenum oxides, containing a small amount of organic from the complexation reaction. The calculated composition is $MoO_3 \cdot 1.0H_2O \cdot 0.3CH_3NH_2$. [12] Structural changes occur gradually as the amorphous aerogel is heated. Heating to 150°C (sample A) causes the evaporation of physically adsorbed water and organic solvents, leaving $MoO_3 \cdot 0.8H_2O$. The rest of the water is chemisorbed and remains in the oxide structure until 350°C. Therefore sample B still retains a small amount ($0<x<0.8$) of chemisorbed H_2O. X-ray diffraction shows that the aerogel is completely dehydrated and crystallized to the orthorhombic phase by 400°C (sample C). Both samples A and B appear amorphous to XRD, showing no characteristic peaks for a crystalline material. (Figure 1)

Infrared spectra for all three samples between 600 - 1100 cm^{-1} are shown in figure 2. Infrared spectroscopy of the amorphous MoO_3 aerogel (sample A) shows broad absorption bands at 700 cm^{-1} and between 850 to 950 cm^{-1}. The 700 cm^{-1} absorption peak is characteristic of the bridging Mo-O-Mo of Mo^{5+}. [15] The broad band, from 850 to 950 cm^{-1}, includes different Mo-O bonds for Mo^{6+}, Mo^{5+}, and even some Mo^{4+}. [15] [16] [17] Spectra of samples B and C are very similar. However, the absorption peaks for sample B are broader and seem to share some absorption peaks with sample A. Samples B and C have a very distinct peak at 1000 cm^{-1} and a smaller peak at 970 cm^{-1}, both are indicative of the Mo=O bond for Mo^{6+}. [18] [19] The broader peaks at 890 and 640 cm^{-1} are those of bridging Mo-O-Mo bonds of Mo^{6+}. [15]

Figure 3 illustrates the XANES at the Mo K-edge of samples A, B, and C, and that of a commercially obtained MoO_3 powder. As has been shown previously, the Mo K-edge XANES is sensitive to changes in the oxidation state and structure of the Mo ion. [20] [21] [22] The pre-edge peak at the onset of the edge (with peak energy near 19995 eV) is due to the transition from the 1s core states to unoccupied 4d states. This transition is dipole forbidden in systems with centrosymmetry and hence it is usually very weak or absent for systems with undistorted octahedral coordination. The extremely strong intensity observed here for the various oxides is due to the large degree of distortion in the local geometry of the first coordination sphere. For systems with a high degree of distortion, this transition becomes dipole allowed due to mixing between p and d states. Within the uncertainty in the data (±0.2eV), the pre-edge peak energy as well as the main edge energy measured at half height are unchanged for the aerogels heat-treated at various temperatures and the commercially obtained crystalline MoO_3 sample. On the basis of the XANES data, it is concluded that the oxidation state of Mo in the aerogels heat-treated at various temperatures is similar to that of Mo in commercially obtained crystalline MoO_3. That is, the oxidation state in the aerogels is +6. It is to be noted that the main edge energy for the various molybdenum oxides (20001.2 eV) is shifted by 8.3 eV relative to that of molybdenum metal (19992.9 eV). The intensity of the pre-edge peak however, increases on going from commercial-

MoO_3 to sample A to sample B and then levels off with further heat treatment (sample C). These changes are likely due to details of the structure within the MO_6 octahedral unit rather than to purely a change in oxidation state. This conclusion is supported by the fact that the pre-edge peak position is unchanged as a function of heat treatment within the uncertainty in the data. The XANES beyond the pre-edge peak for samples B and C are almost identical and are similar to that of the commercial MoO_3 powder. The XANES for sample A, however, shows a slightly different behavior. This part of the spectrum is also sensitive to local geometry beyond the first coordination sphere indicating that the long range order within the first 6 Å for sample A differs from that for the other aerogel samples as will be shown from analysis of the Fourier transform data discussed below.

A comparison of the phase uncorrected Fourier transform of the k^3-weighted Mo K-edge EXAFS for aerogels heat-treated at various temperatures and the commercially obtained MoO_3 powder, is shown in Figure 4. The Fourier transforms display a number of shells with signal above the noise level up to at least 6 Å. The first shell, which is centered near 1.5 Å, consists of single scattering contributions from a complex structure for the Mo-O_6 octahedral unit. For crystalline MoO_3, the first coordination sphere consists of 5 distinct distances, namely, 1.671(x1), 1.734(x1), 1.948(x2), 2.251(x1), and 2.332(x1) Å where the number in parentheses shows the multiplicity for each distance. [23] The second and third shells centered near 3.3 and 5 Å arise mainly from Mo-Mo single scattering contributions with additional contributions from a large number of multiple scattering events. Again, the Fourier transforms for samples B and C are similar and display the first, second and third shell of atoms with no significant change in position indicating a high degree of structural order. In fact, the Fourier transforms for the aerogels heat-treated at 300 and 400 °C display all the shells observed in the Fourier transform for commercially obtained crystalline MoO_3. The peak positions are very similar to those observed for the commercial powder. The only major difference is in the amplitudes of the peaks, which are significantly higher in the Fourier transform of commercially obtained crystalline MoO_3. Meanwhile, sample A shows

a general shift of the maxima positions to smaller radial distances with significantly lower overall intensity. Distances for the aerogel heat-treated at 150 °C appear to be compressed by about 7% relative to that of samples B, C, and commercial MoO_3. On the basis of the Fourier transform data, the degree of order increased on going from sample A to sample B to sample C and then to commercially obtained crystalline MoO_3.

To further elucidate the structure of the aerogels, the local structure parameters such as coordination number (N), distance (R), and disorder (σ^2) for the first shell of atoms were extracted using standard nonlinear fitting procedures. Using the XRD structure data for crystalline MoO_3, three sub-shells with different Mo-O distances were used to model the distorted octahedral structure of the first coordination sphere. Floating parameters were as follows: N_1, N_2, R_1, R_2, R_3, σ_1^2, σ_2^2, and σ_3^2. N_3 was constrained to be equal to 6 - N_1 -N_2. The many body amplitude reduction factor, S_o^2, and the inner potential were determined to be 1.063 (± 0.043) and -7.2 (± 0.5) eV, respectively, from analysis of the first and second coordination spheres of room temperature EXAFS data for metallic Mo. In this analysis, N_1 and N_2 for metallic Mo were constrained to the crystallographic values, which are listed in Table 1. A summary of local structure parameters is also listed in Table 1 for the aerogels heat-treated at various temperatures and commercial MoO_3 powder. The R-factor is a measure of the goodness of the fit. Note that for the aerogel heat treated at 150 °C two samples with significantly different absorption edge jumps were investigated in order to insure that the EXAFS amplitudes are not altered by the thickness [24] or particle size effects [25]. Due to the complexity of the structure of the first coordination sphere and the correlation between coordination numbers and disorders, these results must be interpreted with extreme caution. Our results clearly show that the structure of the first coordination sphere for aerogels heated at 300 and 400 °C as well as commercially obtained crystalline MoO_3 can be approximated by a distorted octahedral coordination, which consists of three distinct distances near 1.71 (x2), 1.95 (x2), and 2.26(x2) Å. The local structure of the first coordination sphere of the aerogel heat-treated at 150 °C, on the other hand, can be

approximated by a distorted octahedral coordination which consists of three distances near 1.73 (x2), 2.08 (x3), and 2.32 (x1) Å.

CV measurements indicate that 1.1 to 1.5 moles of lithium per mole of MoO_3 can be intercalated into the aerogels. (Figure 5, Table 2) However, not all of the initial capacity is reversible. Approximately 72% of the capacity is reversible for sample A while sample B retained 82% of its initial capacity. Sample C exhibited the best reversibility, retaining approximately 90% of the capacity. For each sample, there was no significant capacity change between the 2nd cycle and the 10th cycle. Sample B exhibited the best initial capacity and displays behavior intermediate to that of A and C.

A series of stepwise CV experiments was performed in order to determine the reversibility of the intercalation/de-intercalation peaks. Stepwise CVs for sample A show an irreversible intercalation peak at 2.2 V and a shoulder at 2.55 V. (Figure 6) This lack of reversibility between the OC and 2.2 V region accounts for the low capacity that is retained after the first cycle.

For sample C, there is an irreversible intercalation peak at 2.75 V. (Figure 7) This irreversible peak has also been previously observed in other crystalline MoO_3 materials. [9] This peak appears to be part of an activation process. Cyclic voltammetry sweeps to potentials from OCV to 2.75 V exhibited very limited lithium capacity. However, once this peak is accessed, subsequent cycles show a noticeable increase in capacity in the same region. The peak at 2.3 V is reversible and is deintercalated at 2.45 V on the reverse sweep. This pair of peaks is shifted slightly upon subsequent cycles but retains most of its capacity.

Figure 8 shows a series of CV sweeps for sample B. The intercalation peak at 2.75 V (identical to that of sample C) was irreversible after the first cycle. The intercalation peak at 2.55 V was reversible (de-intercalation at 2.6 V) until intercalation occurred at 2.2 V. This portion of the electrochemical behavior is very similar to that of sample A. Intercalation at this voltage apparently changed the structure so that both intercalation peaks (at 2.55 and 2.2 V) became

irreversible. Subsequent sweeps showed no intercalation peaks. However, capacity is then stabilized at 1.2 Li/Mo.

4. Discussion

The XRD data show that sample C is clearly crystalline with an orthorhombic structure. While both samples A and B appear amorphous from the XRD, the EXAFS and FTIR data provide further insight. From the EXAFS, it is not surprising that sample A exhibits a local environment that is quite different from that of the crystalline sample C. In contrast, sample B is more similar to the crystalline sample C than to the amorphous sample A. This suggests that sample B is nanocrystalline, although the crystallinity does not extend to a large enough scale to be observed by XRD.

The FTIR data show that sample C exhibits peaks that are indicative of bridging Mo-O bonds of Mo^{6+}, with no evidence of Mo in a lower oxidation state. This is not the case for sample A where characteristic peaks for Mo^{5+} and even Mo^{4+} are seen along with Mo^{6+}. It is significant to note that these lower valence peaks are weak and broad, signifying a low concentration. Thus, it is not surprising that the EXAFS data for sample A do not show evidence for Mo^{5+} and Mo^{4+}; instead this suggests that the fraction of these lower valence species in sample A is less than approximately 10% of the total molybdenum content. Although sample B was shown to lack long-range order in the XRD data, its local environment is very similar to that of the crystalline sample C. Both samples B and C exhibit strong absorption peaks for Mo^{6+} with no indication of the lower valence states.

The XANES and RT-EXAFS data for sample C are consistent with the XRD and FTIR results. Namely, sample C has a high degree of structural order with mostly Mo^{6+}, very similar to the commercial MoO_3 powder. The XANES and RT-EXAFS data also show that sample A behaves very differently than sample C. It is assumed that the amorphous material has a more

open structure, contains more oxygen vacancies, and therefore a lower Mo oxidation state. The EXAFS data highlight the structural differences between samples A and C. It is evident that both the long-range and local structure of sample A are unlike that of the crystalline sample C. As discussed above, sample A contains Mo^{5+} and Mo^{4+}; although at relatively low concentrations. Sample B, on the other hand, is practically identical to sample C and very similar to the commercial MoO_3 powder for both the XANES and RT-EXAFS data. Therefore, it can be safely assumed that sample B has a local structure very similar to that of the crystalline sample C. Although XRD detected no long-range order for sample B, the EXAFS and FTIR data show that the material has a local structure similar to the crystalline form, suggesting that sample B is comprised of nanocrystalline MoO_3.

The voltammetric responses are strongly dependent on the form of the MoO_3. This is best shown in comparing the behaviors of samples A and C. Samples A and C displayed two distinctly different CV responses. (Figure 5) The amorphous material exhibited a strong peak at 2.2 V that is irreversible. The crystalline sample, on the other hand, has two peaks, at 2.75 and 2.3 V. In this case it is the low voltage 2.3 V peak which is reversible. This behavior suggests that the Li intercalation processes are markedly different in amorphous and crystalline samples.

The reversible peak at 2.3 V observed for sample C is most likely related to the long range layered structure of the crystalline material. This is because there is no 2.3 V peak observed for sample B, which has short range but no long range order. Both samples A and B show a featureless but very capacitive range between 2.3 and 1.5 V after the first cycle. This is consistent with the presence of disorder in the structure. It has been shown that the amorphous aerogel does not exhibit much of a layered structure, even on the nanometer scale. [12] The disorder means that there will be numerous sites having a large energy spread available to the Li.

The first cycle irreversibility of both the crystalline and amorphous MoO_3 observed in this study was also previously documented. [9] [11] [26] [27] Suggestions for the cause of this irreversibility include structural change, Mo ion migration, and decomposition of H_2O. [9] [26] In

the crystalline sample (C), the activation effect of the peak at 2.75V is indicative of a structural change. Prior work has shown that the interlayer distance almost doubles in crystalline MoO_3 with only a relatively small amount of Li intercalation. [9] The intercalation can effectively disrupt the structure enough to cause local structural change. Moreover, since almost all the water has been driven off by 400°C, it is very unlikely for the irreversibility to be caused by the decomposition of water. The cause for irreversibility in the amorphous material is less obvious. The disappearance of the 2.2V peak can be due to the decomposition of water as well as structural change since it is known that in amorphous MoO_3, dehydration and structural changes are very often coupled. [11] Mo ion migration to Li sites during the first cycle would not explain the activation process of the irreversible peak in sample C nor the large capacitive behavior between 2.3 - 1.5 V after the first cycle in samples A and B.

Sample B was extremely interesting in that it exhibited higher Li capacity compared to either the 150 or the 400°C samples. In addition, the CV response for the 300°C sample displayed characteristics from both the amorphous and the crystalline materials, a reversible shoulder at 2.75 V and an irreversible peak at 2.2 V. This further supports the supposition that sample B is indeed nanocrystalline with long-range disorder. The ability to intercalate in both the crystalline and amorphous sites can be the reason for the higher level of intercalation.

5. Conclusion

Using the sol-gel process, molybdenum oxide aerogels have been produced which are crystalline, nanocrystalline or amorphous depending upon the heat treatment temperature. Through the use of XRD, FTIR, and EXAFS, it has been shown that MoO_3 aerogels heat treated to 300 °C are crystalline at the nanoscale while maintaining long range disorder. Stepwise CV was used to characterize the reversible and irreversible electrochemical responses for the different materials. The first cycle irreversibility in the crystalline material is most likely due to local structural change. The cause for the first cycle irreversibility for the amorphous material is not as

clear as both structural change and the decomposition of water are likely to contribute. The nanocrystalline sample exhibits electrochemical characteristics similar to both the crystalline and amorphous samples and, interestingly, intercalates greater amounts of lithium than either form.

6. Acknowledgments

The authors acknowledge financial support by ONR. ANM also acknowledges financial support by the Carderock Division of the Naval Surface Warfare Center's In-house Laboratory Independent Research Program sponsored by ONR administered under Program Element 0601152N. The support of the U.S. DOE under Contract # DE-AS05-80-ER-10742 for its role in the development and operation of beam line X-11A at NSLS is also acknowledged. The NSLS is supported by the U.S. DOE under Contract # DE-AC02-76CH00016.

References

1. G.A. Nazri and C. Julien, Solid State Ionics, 68 (1994) 111.
2. K. Hinokuma, A. Kishimoto, and T. Kudo, J. Electrochem. Soc., 141 (1994) 876.
3. J.O. Besenhard, J.Heydecke, E. Wudy, H.P. Fritz, and W. Foag, Solid State Ionics, 8 (1983) 61.
4. C. Julien, G.A. Nazri, J.P. Guesdon, A.Khelfa, and O.M. Hussain, Solid State Ionics, 73 (1994) 319.
5. T. C. Arnoldussen, J. Electrochem. Soc., 123 (1976) 527.
6. J.P. Pereira-Ramos, N. Kumagai, and N. Kumagai, J. Power Sources, 56 (1995) 87.
7. B. Yebka and C. Julien, Mater. Res. Soc. Symp. Proc., 369 (1995) 119.
8. M. Sugawara, Y. Kitada, and K. Matsuki, J. Power Sources, 26 (1989) 373.
9. T. Tsumura and M. Inagaki, Solid State Ionics, 104 (1997) 183.
10. W. Dong and B. Dunn, J. Am. Ceram. Soc., in press.
11. F. Bonino, L. Peraldo Bicelli, B. Rivolta, M. Lazzari, and F. Festorazzi, Solid State Ionics, 17 (1985) 21.
12. W. Dong and B. Dunn, J. Mat. Chem., 8 (1998) 665.
13. D. E. Sayers, S. M. Heald, M. A. Pick, J. I. Budnick, E. A. Stern, and J. Wong, Nucl. Instrum. Methods Phys. Res., 208 (1983) 631.
14. E.A. Stern, Phys. Rev. B, 48 (1993) 9825.
15. N. Mizuno, K. Katamura, Y. Yoneda, and M. Misono, J. Catal., 83 (1983) 384.
16. C.R. Deltcheff, R. Thouvenot, and M. Fouassier, Inorg. Chem., 21 (1982) 30.
17. R.M. Silverstein, G.C. Bassler, and T.C. Morrill, Spectrometric

Identification of Organic Compounds, John Wiley & Sons, New York, 4th ed. (1981), 95.

18. M. Akimoto and E. Echigoya, Chem. Lett., 645 (1978) 1183.

19. T. Tsai, K. Maruya, M. Ai, and A. Ozaki, Bull. Chem. Soc. Jpn., 55 (1982) 949.

20. G.N. George, C.A. Kipke, R.C. Prince, R.A. Sunde, J.H. Enemark, and S.P. Cramer, Biochemistry, 28 (1989) 5075.

21. M. R. Antonio, R. G. Teller, D. R. Sandstrom, M. M. Mehicic, and J. F. Brazdil, J. Phys. Chem., 92 (1988) 2939.

22. M. R. Antonio, J. F. Brazdil, L. C. Glaeser, M. Mehicic, and R. G. Teller, J. Phys. Chem., 92 (1988) 2338.

23. P. Villars and L.D. Calver, Pearson's Handbook of Crystallographic Data for Intermetallic Phases, American Society for Metals, Metals Park, OH, vol. 3, (1985), p. 2756.

24. E. A. Stern and K. Kim, Phys. Rev. B, 23 (1981) 3781.

25. K.-Q. Lu and E. A. Stern, Nucl. Instrum. Methods Phys. Res., 208 (1983) 631.

26. H. Kobayashi, M. Tabuchi, M. Shikano, Y. Nishimura, H. Kageyama, T. Ishida, H. Nakamura, Y. Kurioka, and R. Kanno, J. Power Sources, 81-82 (1999) 524.

27. A. Yu, N. Kumagai, Z. Liu, and J.Y. Lee, Solid State Ionics, 106 (1998) 11.

Figure Captions

1. XRD of samples A, B, and C. Samples A and B appear amorphous while sample C is orthorhombic. The peaks up to $2\theta = 50$ are indexed.
2. FTIR spectra of samples A, B, and C. Sample A shows the presence of valences other than Mo^{6+} (700, 850 – 950 cm^{-1}), with no Mo=O bonds. Samples B and C show very distinct Mo=O bonds (1000 cm^{-1}) with mostly Mo^{6+} behavior.
3. XANES of MoO_3 aerogels subjected to various heat treatements, as compared to a commercially obtained crystalline MoO_3 and elemental Mo.
4. Room temperature EXAFS of MoO_3 aerogels subjected to various heat treatments, as compared to a commercially obtained crystalline MoO_3.
5. First cycle cyclic voltammetry for samples A, B, and C.
6. Stepwise CV for sample A. Cycles range from OCV = 3.2 V to 1) 2.8 V, 2) 2.3 V, 3) 2.1 V, 4) 1.9 V, and 5) 1.5 V.
7. Stepwise CV for sample C. Cycles range from OCV = 3.3 V to 1) 2.6 V, 2) 2.5 V, 3) 2.4 V, 4) 2.2 V, 5) 2.0 V, and 6) 1.5 V.
8. Stepwise CV for sample B. Cycles range from OCV = 3.2 V to 1) 2.8 V, 2) 2.3 V, 3) 2.1 V, 4) 2.0 V, and 5) 1.5 V.

Table 1. Summary of local structure parameters for aerogel molybdenum oxides (MoO_3).*

Sample	EXAFS Temp.	Δμx	N	R (X)	Av. R (Å)	σ^2 ($10^{-3}X^2$)	R-factor
Mo	RT	1.1	8.0	2.729 ± 0.002		4.2 ± 0.2	0.0048
			6.0	3.148 ± 0.002		4.3 ± 0.2	
Cmmercial-MoO_3	RT	1.2	2.1 ± 0.2	1.716 ± 0.003		4.4 ± 0.8	0.0010
			2.6 ± 0.2	1.950 ± 0.002	1.937	2.7 ± 0.5	
			1.3	2.268 ± 0.008		4.2 ± 1.2	
Commercial-MoO_3	LN	1.2	2.3 ± 0.7	1.720 ± 0.009		5.7 ± 2.4	0.0046
			2.2 ± 0.3	1.947 ± 0.004	1.939	0.9 ± 0.9	
			1.5	2.262 ± 0.016		3.7 ± 2.5	
Aerogel-MoO_3 (150 °C)	RT	2.4	2.2 ± 0.6	1.731 ± 0.008		3.7 ± 1.5	0.0135
			2.8 ± 1.1	2.013 ± 0.024	1.951	10.3 ± 6.5	
			1.0	2.317 ± 0.058		8.0 ± 13.2	
Aerogel-MoO_3 (150 °C)	LN	2.4	2.2 ± 0.2	1.729 ± 0.003		3.9 ± 0.6	0.0023
			3.2 ± 0.3	2.018 ± 0.010	1.944	13.4 ± 2.5	
			0.6	2.321 ± 0.0148		2.7 ± 2.7	
Aerogel-MoO_3 (150 °C)	LN	0.43	1.9 ± 0.7	1.724 ± 0.012		3.9 ± 2.0	0.0272
			3.3 ± 1.3	2.021 ± 0.038	1.968	16.3 ± 12.2	
			0.8	2.332 ± 0.064		5.6 ± 12.5	
Aerogel -MoO_3 (300 C)	RT	0.64	2.2 ± 0.5	1.710 ± 0.006		5.0 ± 1.5	0.0053
			1.8 ± 0.4	1.954 ± 0.005	1.968	2.4 ± 1.1	
			2.0	2.263 ± 0.022		8.9 ± 3.7	
Aerogel -MoO_3 (400 C)	RT	0.55	1.8 ± 0.5	1.709 ± 0.008		3.8 ± 1.7	0.0091
			2.1 ± 0.5	1.961 ± 0.008	1.996	4.1 ± 1.8	
			2.1	2.278 ± 0.023		8.3 ± 4.0	
Aerogel -MoO_3 (400 C)	LN	0.56	1.8 ± 0.6	1.705 ± 0.008		3.7 ± 1.8	0.0082
			2.0 ± 0.4	1.953 ± 0.007	1.998	2.6 ± 1.4	
			2.2	2.261 ± 0.020		6.9 ± 3.2	

* Aerogel samples are heat-treated at 150, 300, and 400 °C. A commercially obtained sample of crystalline MoO_3 (Alfa-Aesar) is included for comparison. The weighted average for the Mo-O distances (i.e., $\sum N_i R_i / \sum N_i$) is also listed as Av. R.

Table 2: Intercalation properties of MoO_3 aerogels compared to literature values.

MoO_3	Li/Mo	mAh/g
Sample A (150 °C)	1.2	240
Sample B (300 °C)	1.5	280
Sample C (400 °C)	1.1	210
Crystalline [26]	1.2	200
Amorphous [11]	1.5	260

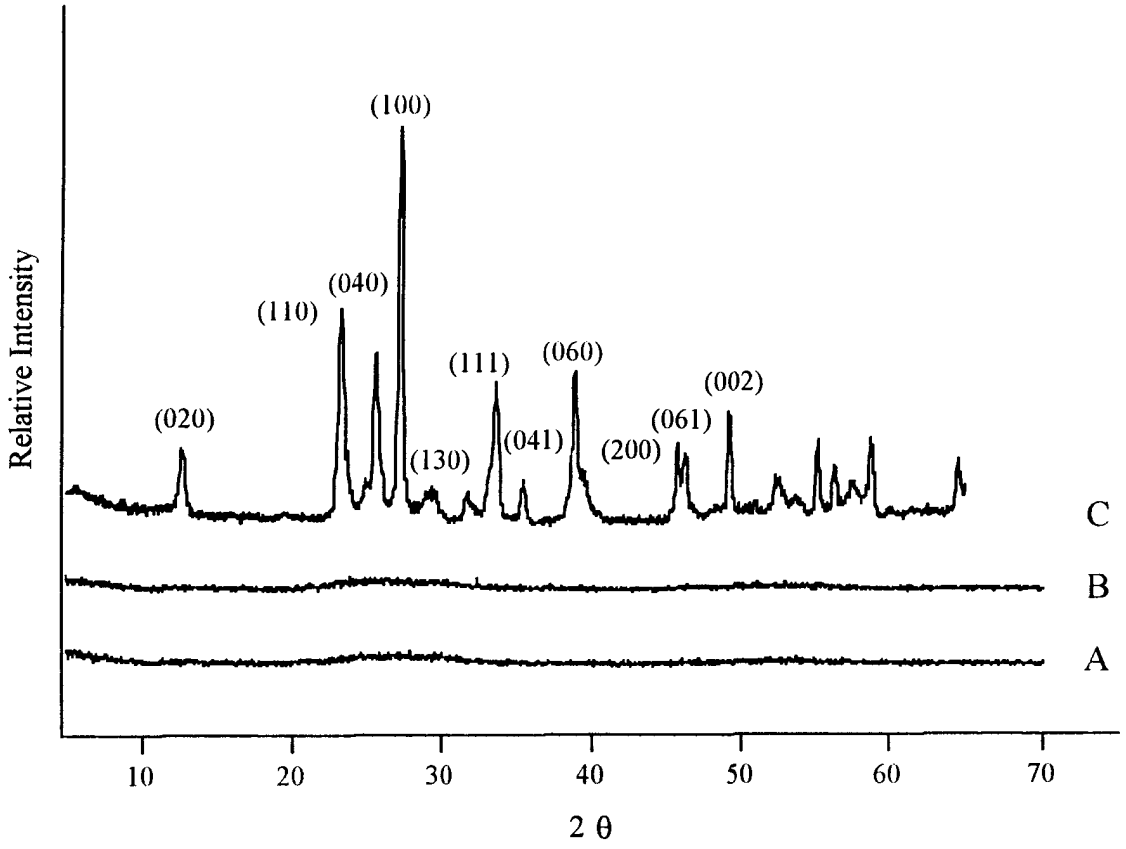
Relative Intensity
(100)
(110)
(040)
(020)
(111)
(060)
(002)
(061)
(041)
(130)
(200)
C
B
A
10
20
30
40
50
60
70
2 θ

Figure 1

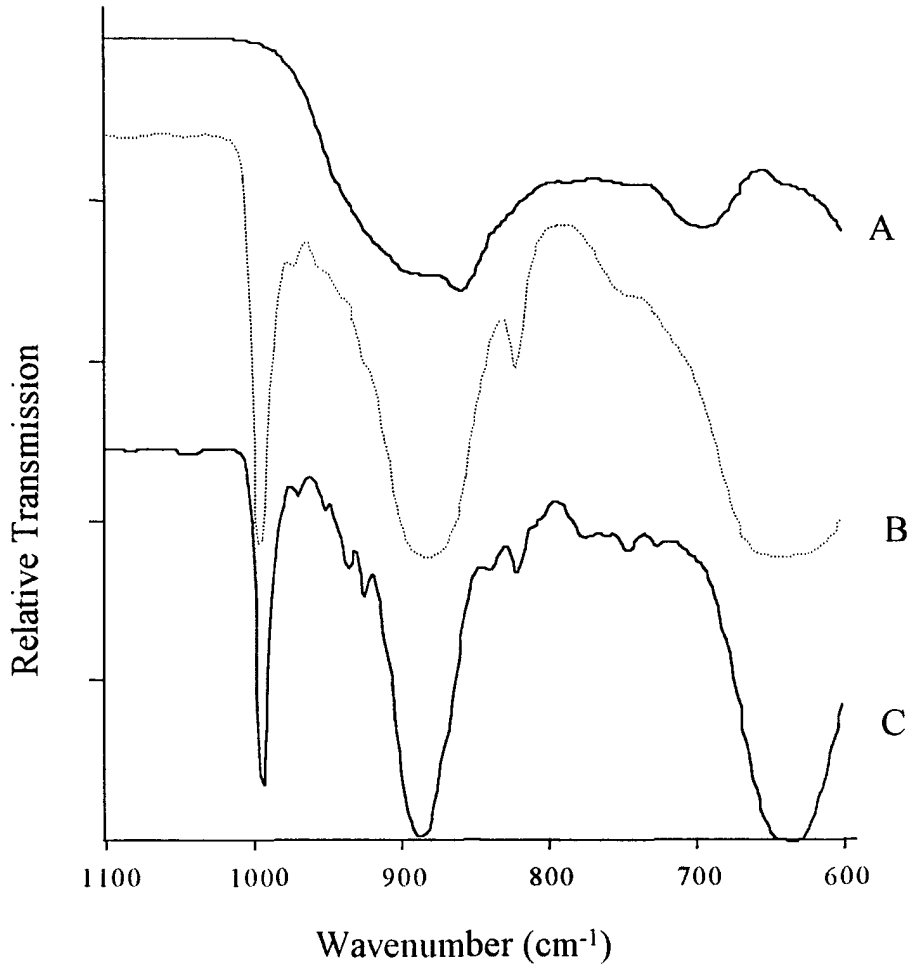
Relative Transmission
A
B
C
1100
1000
900
800
700
600
Wavenumber (cm-1)

Figure 2

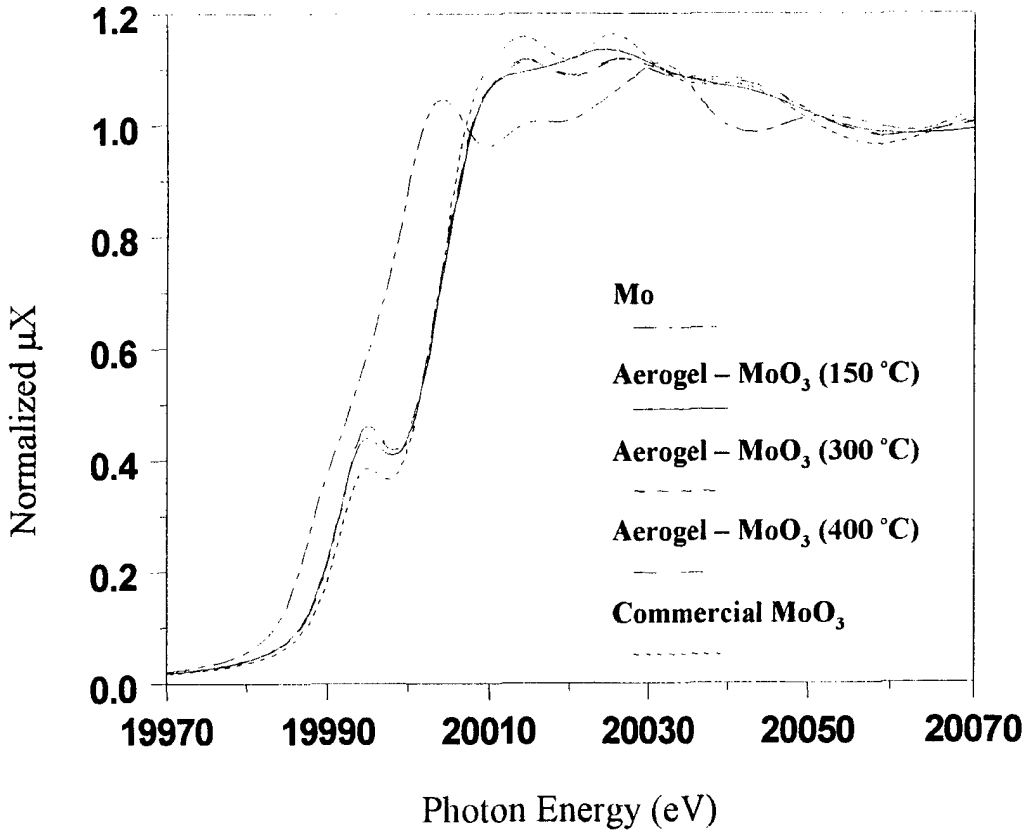
1.2
1.0
0.8
0.6
0.4
0.2
0.0
Normalized μX
19970
19990
20010
20030
20050
20070
Photon Energy (eV)
Mo
Aerogel – MoO3 (150 °C)
Aerogel – MoO3 (300 °C)
Aerogel – MoO3 (400 °C)
Commercial MoO3

Figure 3.

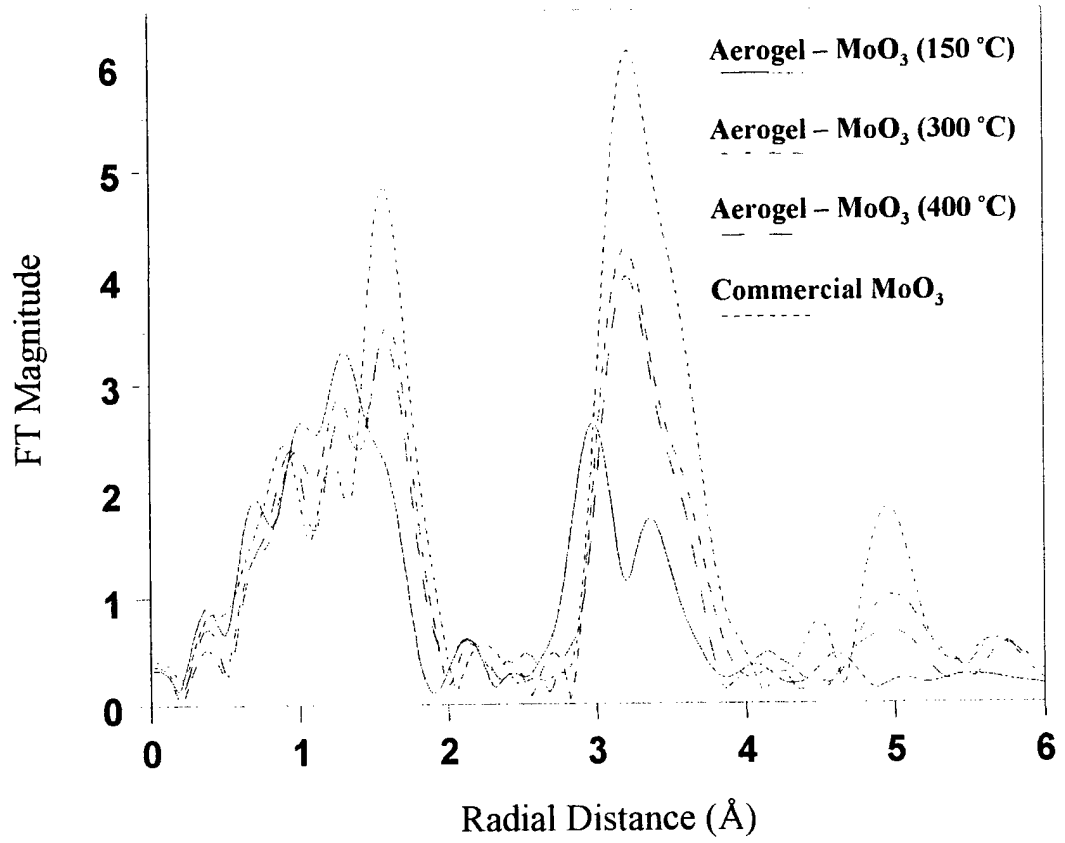
Aerogel – MoO_3 (150 °C)
Aerogel – MoO_3 (300 °C)
Aerogel – MoO_3 (400 °C)
Commercial MoO_3
FT Magnitude
Radial Distance (Å)
0
1
2
3
4
5
6

Figure 4

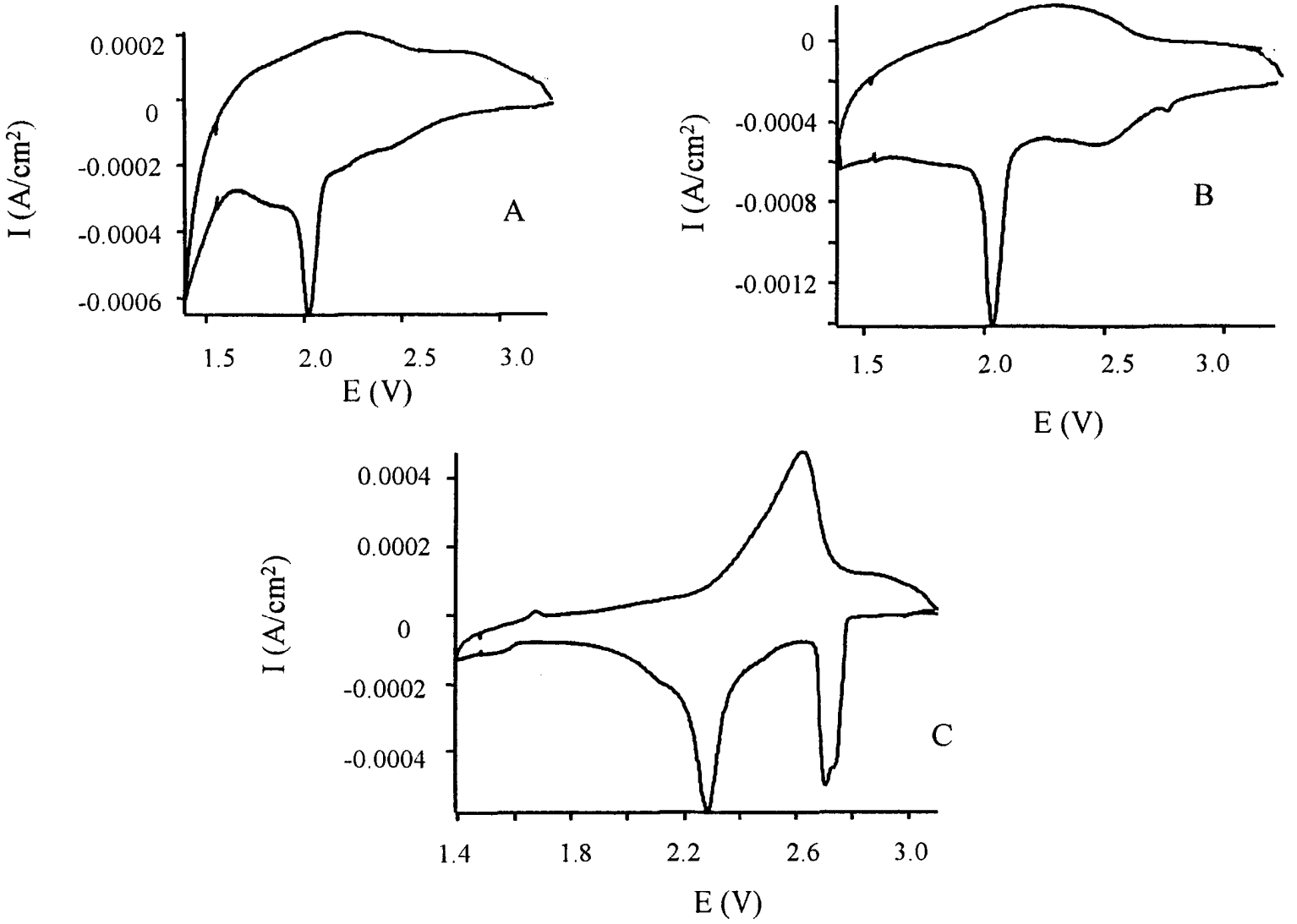
0.0002
0
-0.0002
-0.0004
-0.0006
I (A/cm²)
1.5
2.0
2.5
3.0
E (V)
A
0
-0.0004
-0.0008
-0.0012
I (A/cm²)
1.5
2.0
2.5
3.0
E (V)
B
0.0004
0.0002
0
-0.0002
-0.0004
I (A/cm²)
1.4
1.8
2.2
2.6
3.0
E (V)
C

Figure 5

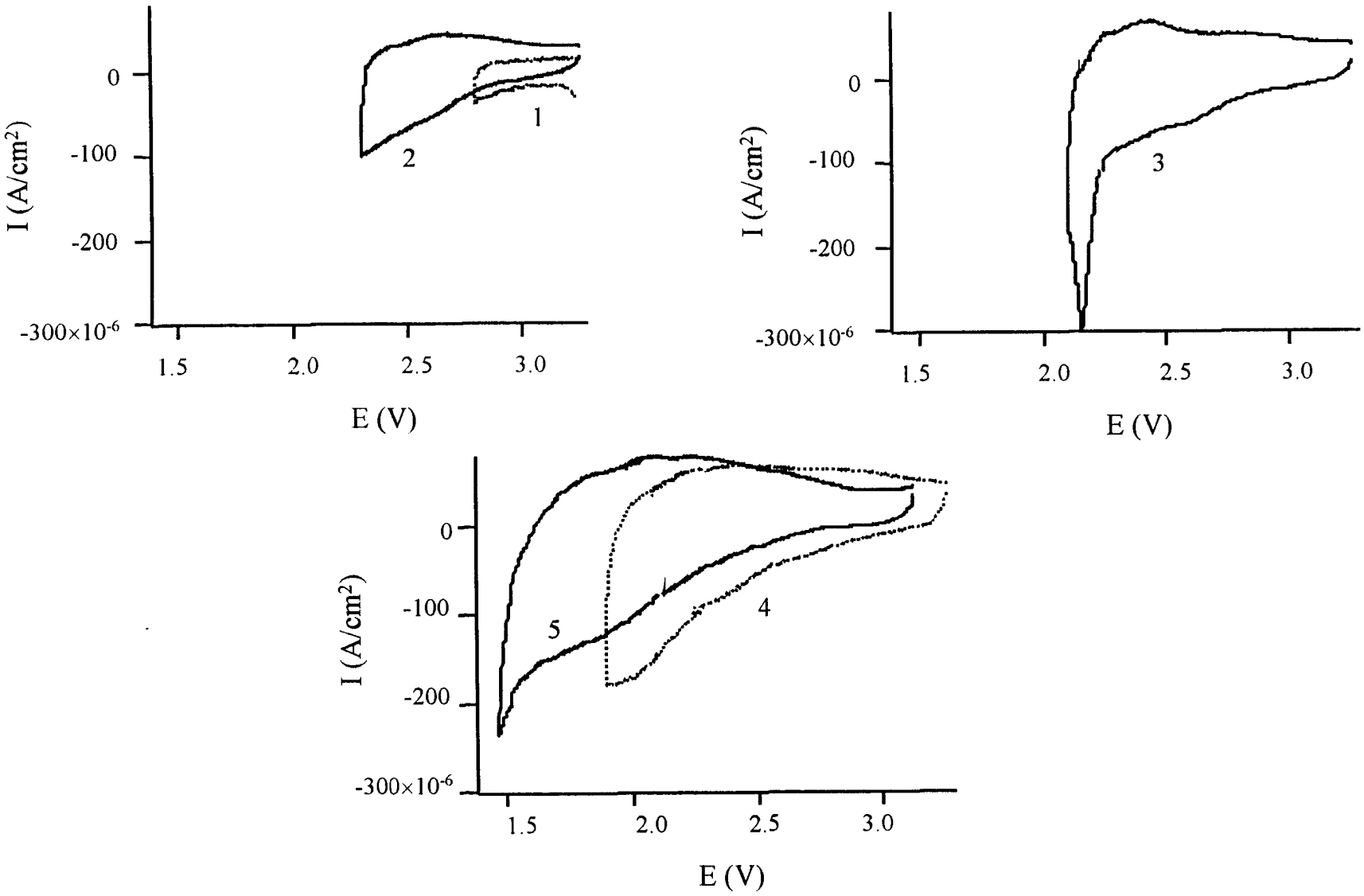

Figure 6

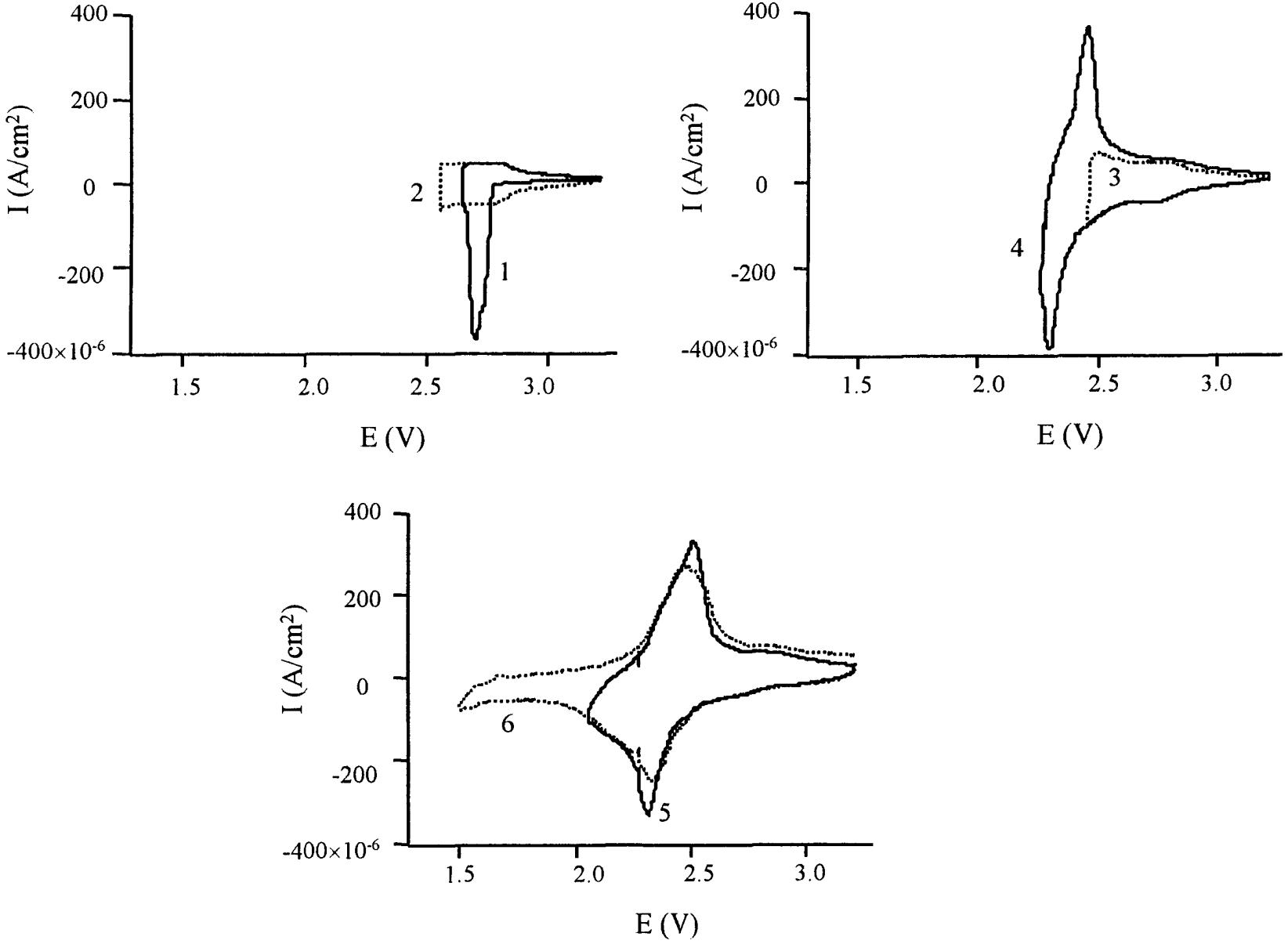

Figure 7

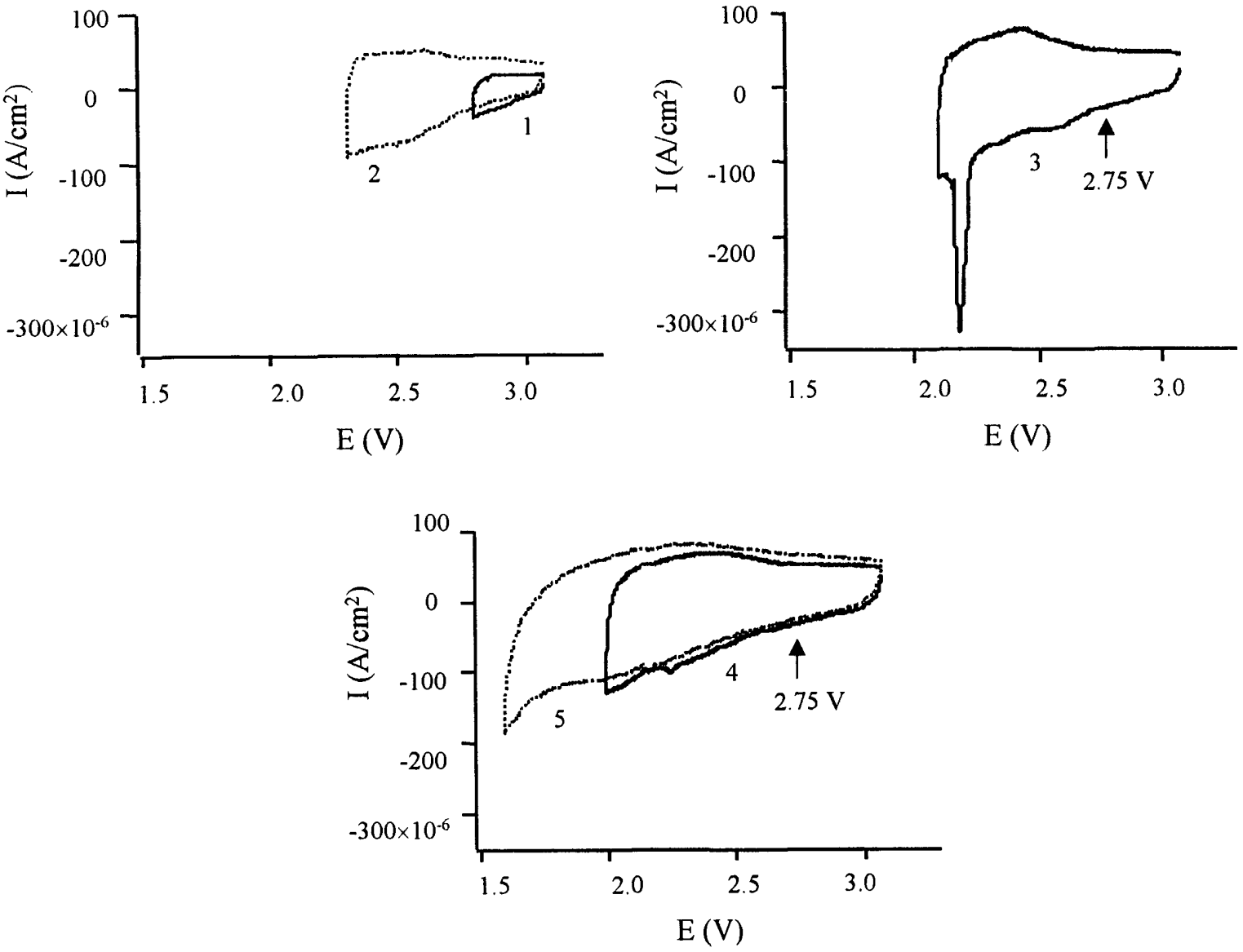

Figure 8